JAAS

ROYAL SOCIETY OF CHEMISTRY

PAPER

View Article Online
View Journal | View Issue

Check for updates

Cite this: J. Anal. At. Spectrom., 2023, 38, 1652

Multiple-element analysis of coal using collinear double-pulse laser-induced breakdown spectroscopy

Qi Ni,[b] Yong He,[ab] Wubin Weng,[b] Yanqun Zhu[ab] and Zhihua Wang *[ab]

Collinear double-pulse laser-induced breakdown spectroscopy has been developed to enhance the emission signal of coal plasma. The influence of the energy ratio and the inter-pulse delay time on the intensity enhancement factors of the emission lines of representative elements in coal (*i.e.* carbon, hydrogen, oxygen, together with some metal elements such as iron, calcium, sodium and potassium) was investigated. The results showed that the collinear double-pulse configuration could sufficiently enhance the emission signals with an optimized inter-pulse delay time and energy ratio, and significant intensity enhancement factors were achieved for most of the selected lines with an energy ratio of 20 : 100. Meanwhile, the correlation between the signal enhancement and the upper energy level was investigated using neutral and ionic calcium lines. Finally, the plasma temperature, lifetime and morphology were calculated and observed to better explain the enhancement mechanism with different energy ratios and inter-pulse delay times.

Received 4th June 2023
Accepted 23rd June 2023

DOI: 10.1039/d3ja00180f

rsc.li/jaas

Published on 26 June 2023. Downloaded by Zhejiang University on 11/8/2023 7:15:22 AM.

1. Introduction

Coal is one of the primary fossil fuels, consisting mainly of carbon, hydrogen, oxygen, nitrogen and sulfur, together with inorganic impurities such as iron, calcium, sodium and potassium. As coal is one of the main fuel sources used in thermal power plants, the rapid and accurate measurement of the elemental composition, calorific value, moisture content, alkali metal content and some other properties of coal is extremely useful for online optimization of the operation of coal-fired power plants. Traditional techniques for the ultimate analysis and proximate analysis of coal, such as X-ray fluorescence (XRF), thermogravimetric analysis (TGA) and inductively coupled plasma mass spectrometry (ICP-MS), have limitations in the detection of low-atomic-number elements or are time-consuming. Laser-induced breakdown spectroscopy (LIBS) has been proposed and demonstrated as a potential technique to provide rapid, real-time and multi-element detection of materials.[1–3] The elemental species and content can be analyzed from the line wavelength and intensities.

However, the emission intensity of some non-metallic elements and trace elements is usually too weak to be detected, which leads to insufficient sensitivity of LIBS technology. Therefore, many configurations have been proposed to enhance the emission signal of plasma and improve the detection sensitivity of LIBS, mainly including the double-pulse LIBS,[4–7] spatially confined LIBS,[8,9] and magnetic-field enhanced LIBS.[10–13] In recent years, a lot of work has been done on double-pulse LIBS. Compared to other methods used to improve the LIBS performance, the double-pulse LIBS configuration is relatively simple with a significant enhancement of the plasma emission spectrum.

Two main beam geometries are used in double-pulse LIBS: orthogonal and collinear. In collinear double-pulse LIBS, two laser pulses are focused orthogonally at the same point on the sample surface with the same axis propagation. In orthogonal double-pulse LIBS, one laser pulse is perpendicular to the sample surface and the other is parallel to it. Collinear double-pulse LIBS is much easier to set up and requires less space than orthogonal double-pulse LIBS. In double-pulse LIBS, the wavelength, pulse width, energy ratio, inter-pulse delay time, ambient atmosphere and the angle of incidence of the two pulses are important parameters that can directly influence the plasma characteristics.[14,15] The intensity enhancement, signal-to-noise ratio, signal-to-background ratio and detection limit were monitored to evaluate the performance of double-pulse LIBS.[16]

Despite the improved performance of double-pulse LIBS, the signal intensity enhancement mechanism is also studied. Possible enhancement mechanisms proposed mainly include the pulse–plasma coupling effect and the pulse–target interaction.[17] The first laser pulse can effectively change the atmospheric conditions around the sample surface and improve the sample temperature, resulting in an increased mass ablation.[18] The second laser pulse can also reheat the plasma plume

[a]Qingshanhu Energy Research Center, Zhejiang University, 311300, Hangzhou, China. E-mail: wangzh@zju.edu.cn

[b]State Key Laboratory of Clean Energy Utilization, Zhejiang University, 310027, Hangzhou, China

This journal is © The Royal Society of Chemistry 2023

Published on 26 June 2023. Downloaded by Zhejiang University on 11/8/2023 7:15:22 AM.

generated by the first laser pulse or ablated more mass.[19] The signal intensity enhancement mechanism is complicated with different configurations and experimental conditions. Plasma temperature, plasma lifetime, ablated mass and plasma volume have been used to explain the enhancement mechanism.[20,21]

Numerous studies have been carried out on coal analysis using laser-induced breakdown spectroscopy. Both the ultimate analysis and proximate analysis of coal using LIBS are presented and different calibration models are proposed to improve the prediction accuracy of LIBS. Ma *et al.* used double-pulse laser-induced breakdown spectroscopy to detect the sulfur concentration of coal, and the sulfur spectral intensity was found to be enhanced by 2.3 times.[22] On the other hand, S. Legnaioli, et al. used the collinear double-pulse LIBS system combing with the ANN model for the online monitoring of ash content and obtained an absolute precision better than ±4% w%.[23] However, few studies have focused on the simultaneous multi-element detection of coal using collinear double-pulse LIBS. The similarities and differences in the intensity enhancement factors, optimized experimental parameters and the enhancement mechanisms of organic and metal elements are also insufficiently studied in collinear double-pulse LIBS.

In this study, collinear double-pulse laser-induced breakdown spectroscopy was developed for the multi-element detection of coal samples. The representative spectral lines of carbon, hydrogen, oxygen, along with some metal elements such as iron, calcium, sodium, magnesium and potassium were analyzed. The intensity enhancement factor with different inter-pulse delay time (range from 0–32 μs) and energy ratios (range from 5 : 115 to 80 : 40) was discussed, and the signal-to-background (S/B) and signal-to-noise (S/N) ratios of carbon and hydrogen at the optimized energy ratio were compared with those of single-pulse LIBS. The neutral and ionic calcium lines were chosen to observe the correlation between the intensity enhancement factor and the energy level. The plasma temperature, lifetime and morphology were observed to better explain the signal intensity enhancement mechanism.

2. Experimental setup

The collinear double-pulse LIBS experimental setup is illustrated in Fig. 1. Two collinear laser beams were generated and aligned into the same beam path inside the double pulse Nd:YAG laser (Vlite 300, Beamtech). The two pulses were perpendicular to the sample surface and operated both at 532 nm with a pulse width of 8 ns, and a repetition frequency of 1 Hz. The inter-pulse delay time of the two laser pulses was adjusted using a digital delay generator (DG645, Stanford Research Systems). The laser beams were focused on the surface of the coal samples by a convex lens with a focal length of 150 mm, and the emission signal of the plasma was collected by an off-axis parabolic mirror with through holes (MPD229H-F01, Thorlabs) and coupled into a spectrometer (Aryelle Butterfly, LTB) equipped with an electron-multiplying charge coupled device (EMCCD, Andor). The spectrometer had two channels: the UV channel and the VIS channel. The UV channel had a wavelength range of 190–350 nm with a high spectral resolution of 12 pm, and the VIS channel had a wide wavelength range of 350–950 nm with a spectral resolution of 36 pm. Highly purified helium (99.99%) was used as a purge gas at a flow rate of 1 L min^{-1} to avoid unwanted chemical reactions with air.

To reduce the matrix effect, the coal sample was air-dried, crushed, and sieved to a size of 100 mesh, then the coal powder was pressed into pellets with a diameter of 20 mm using a hydraulic press. The prepared coal sample was placed on a rotating stage. To increase the repeatability, the measurements were taken at 5 different ablation points and the emission signals were accumulated to form one spectrum. For each experiment, 3 spectra were taken and the average of which was used as the final spectrum.

For the single-pulse LIBS measurement, the pulse energy was fixed at 120 mJ, and the delay time between the laser pulse and the beginning of the spectrum acquisition was 0.8 μs. For the double-pulse LIBS measurement, the energy of the first pulse and the second pulse was E_1 and E_2, respectively, and the energy

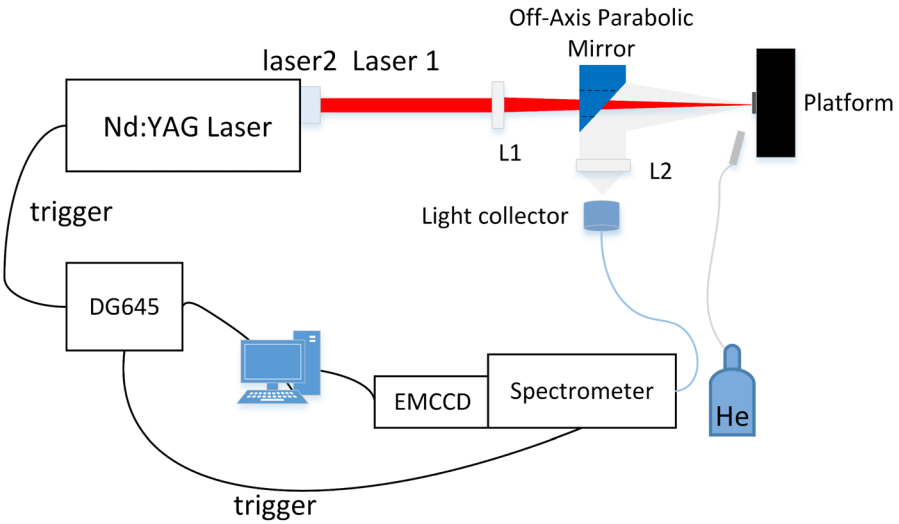

Fig. 1 Schematic diagram of double-pulse LIBS.

Published on 26 June 2023. Downloaded by Zhejiang University on 11/8/2023 7:15:22 AM.

ratio changed continuously from 5 : 115 ($E_1 = 5$ mJ and $E_2 = 115$ mJ) to 80 : 40 ($E_1 = 80$ mJ and $E_2 = 40$ mJ) with the total energy remaining $E_1 + E_2 = 120$ mJ. The detection delay time was set to 0.8 μs after the second pulse. The inter-pulse delay time was adjusted by the DG645 changing from 0 μs to 32 μs.

In the experiment, the influence of the energy ratio and inter-pulse delay time on the signal intensity enhancement was investigated, and the optimized inter-pulse delay time and energy ratio of double-pulse LIBS were obtained to get the maximum plasma emission signal. The degree of intensity enhancement by double-pulse LIBS was expressed by the intensity enhancement factor, which is the ratio of the intensities of the selected spectral lines in double-pulse LIBS to that in single-pulse LIBS.

3. Results and discussion

3.1 Comparison of single-pulse and double-pulse LIBS spectra

The parametric study (*i.e.* energy ratio, inter-pulse delay time) of collinear double-pulse LIBS was carried out on Mongolian coal containing 63.38% of C, 3.3% of H and 12.7% of O by air dry base. The typical spectra of single-pulse LIBS and double-pulse LIBS under the optimized condition (*i.e.* inter-pulse delay time of 0.2 μs, energy ratio of 20 : 100 and detection delay time of 0.8 μs) are shown in Fig. 2. The double-pulse LIBS spectrum showed an obvious signal intensity enhancement compared to the spectrum of single-pulse LIBS. The C I 247.86 nm line in the spectral range of 0–350 nm and the H I 656.27 nm line in the spectral range of 350–950 nm were used to illustrate the intensity enhancement. The observed intensity enhancement factor of the C I 247.86 nm and H I 656.27 nm lines was approximately 2.3 and 2.5, respectively. In addition, the full width at half maximum (FWHM) of the lines was determined by the numerical fitting of a Lorentzian profile. The line width (FWHM) of the C I 247.86 nm and H I 656.27 nm lines were 0.037 nm and 1.1 nm in the single-pulse LIBS spectrum, respectively, which was smaller than 0.044 nm and 1.8 nm in the double-pulse LIBS spectrum. The double-pulse configuration had a significant effect on both the line broadening and peak intensity of the LIBS spectrum.

To better describe the signal quality, the signal intensity, signal-to-background (S/B) and signal-to-noise (S/N) ratios of the C I 247.86 nm and H I 656.27 nm lines as a function of inter-pulse delay time are shown in Fig. 3. The black and red dashed lines show the corresponding values of C I 247.86 nm and H I 656.27 nm lines in single-pulse LIBS, respectively. The S/B ratio showed a consistent trend with the signal intensity for both spectral lines. A significant intensity enhancement of the C I

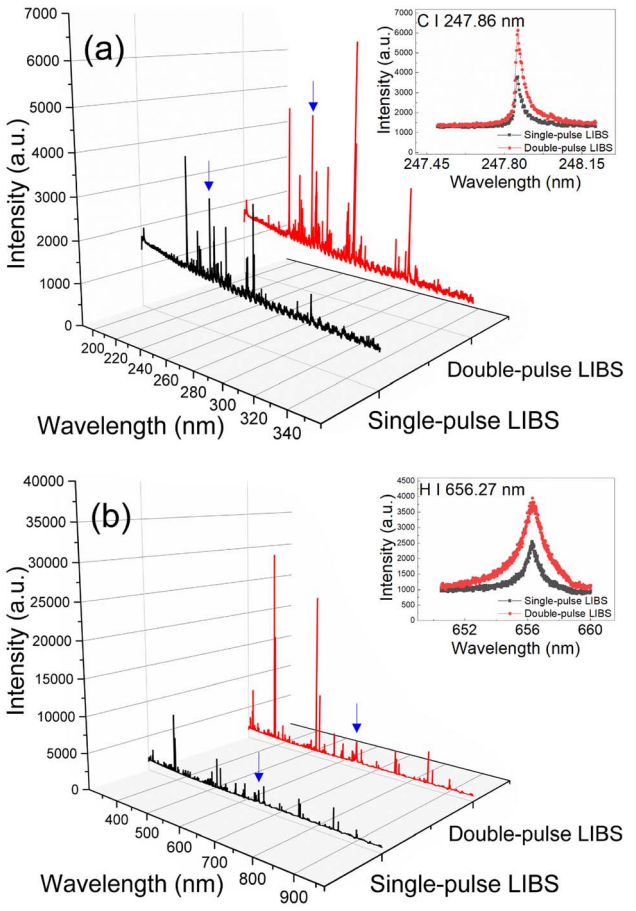

Fig. 2 LIBS spectra of coal plasma in (a) 190–350 nm and (b) 350–950 nm, were obtained using single-pulse LIBS (black) and double-pulse LIBS (red).

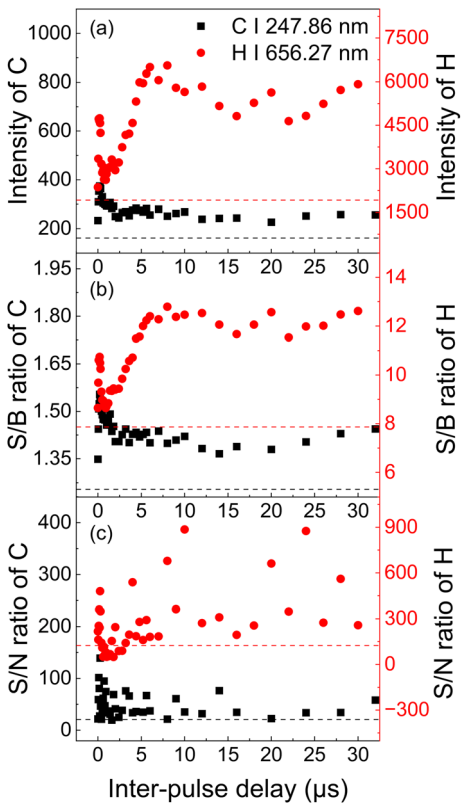

Fig. 3 (a) Observed intensity, (b) S/B ratio and (c) S/N ratio as a function of inter-pulse delay time for C I 247.86 nm and H I 656.27 nm lines in single-pulse LIBS and double-pulse LIBS (energy ratio of 20 : 100).

This journal is © The Royal Society of Chemistry 2023

Published on 26 June 2023. Downloaded by Zhejiang University on 11/8/2023 7:15:22 AM.

247.86 nm and H I 656.27 nm lines was found with the inter-pulse delay time of 0.2 μs and 6 μs. For the C I 247.86 nm line, the S/B and S/N ratios of the double-pulse LIBS were 1.6 and 27.6 at an inter-pulse delay time of 0.2 μs, respectively, which were 1.2 and 1.3 times higher than those of the single-pulse LIBS. For the H I 656.27 nm line, the S/B and S/N ratios of the double-pulse LIBS were 12.4 and 181.3 at an inter-pulse delay time of 6 μs, respectively, which were 1.6 and 1.5 times higher than those of the single-pulse LIBS. The results indicated that the double-pulse configuration was useful for improving the quality of the emission signal.

3.2 Influence of energy ratio and inter-pulse delay on signal enhancement

To better study the enhancement effect of collinear double-pulse LIBS, the intensity enhancement factor of spectral lines of selected elements with different energy ratios and inter-pulse delay time was measured and compared. Several representative neutral and ionic lines in the spectral range of 190–950 nm were selected according to the NIST database, including spectral lines of carbon, hydrogen, oxygen, and the alkali metal elements of sodium and potassium, which were essential for the elemental analysis of coal.

The content of carbon, hydrogen and oxygen plays a decisive role in the elemental analysis of coal. In the first part of this work, the influence of the energy ratio and inter-pulse delay time on the emission lines of the major elements of coal (*i.e.* C I 247.86 nm, H I 656.27 nm and O I 777.42 nm) was investigated. The intensity enhancement factors of the spectral lines as a function of inter-pulse delay time at different energy ratios are shown in Fig. 4. For energy ratios above and below 40 : 80, the enhancement curves differed significantly. A greater enhancement was achieved when the energy of the first laser pulse was lower than that of the second laser pulse (*i.e.* energy ratios of 20 : 100, 10 : 110 and 5 : 115). In addition, high intensity enhancement of all three spectral lines was achieved with an energy ratio of 20 : 100. There were two obvious peaks in intensity enhancement curves at an energy ratio of 20 : 100. The largest intensity enhancement factor of the C I 247.86 nm line was 2.3 at the first peak with an inter-pulse delay time of 0.2 μs. Meanwhile, the largest intensity enhancement factors of H I 656.27 nm and O I 777.42 nm were found to be 3.4 and 5.9 respectively at the second peak with an inter-pulse delay time of 8 μs.

3.3 Effects of inter-pulse delay on the signal enhancement of metallic lines

The intensity enhancement factor of the spectral lines of metallic elements (*i.e.* Fe, Mg, Ca, Na, K) was also investigated with the optimized energy ratio of 20 : 100. The intensity enhancement factors of the Fe II 259.94, Mg II 279.55 nm, Ca II 393.37 nm, Na I 589.59 nm and K I 769.90 nm lines changing with the inter-pulse delay time are shown in Fig. 5. The observed trends were similar to the emission lines mentioned above. Two peak enhancement factors were also observed for the curves of the metallic lines with increasing inter-pulse delay time. The

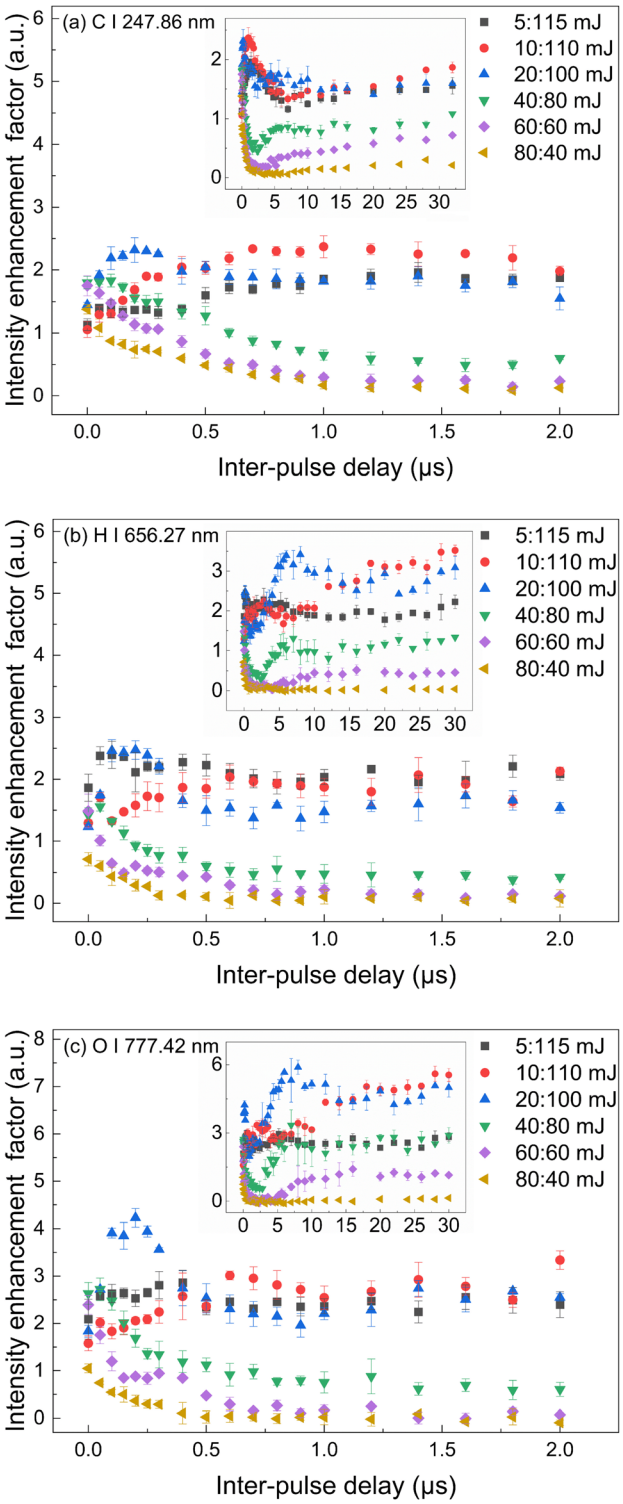

Fig. 4 Distribution of intensity enhancement factor as a function of inter-pulse delay time for different energy ratios: (a) C I 247.86 nm, (b) H I 656.27 nm and (c) O I 777.42 nm.

two peak intensity enhancement factors of the Fe II 259.94 nm, Mg II 279.55 nm and Ca II 393.37 nm lines were found with the inter-pulse delay time of about 0.2 μs and 5 μs. The ionic emissions of the Ca II 393.37 nm line showed significantly

Published on 26 June 2023. Downloaded by Zhejiang University on 11/8/2023 7:15:22 AM.

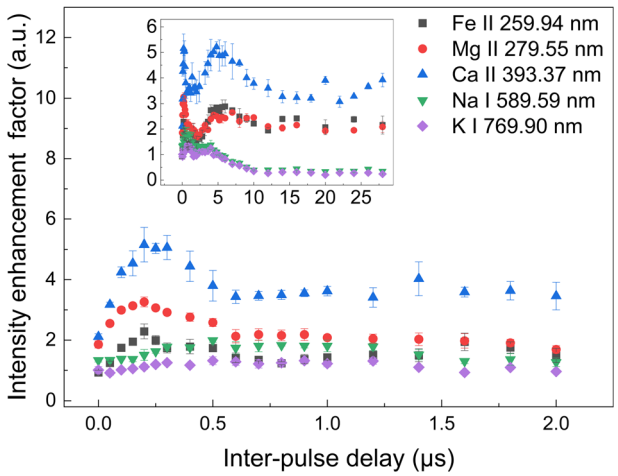

Fig. 5 The intensity enhancement factor of the spectral lines of selected metallic elements with increasing inter-pulse delay time.

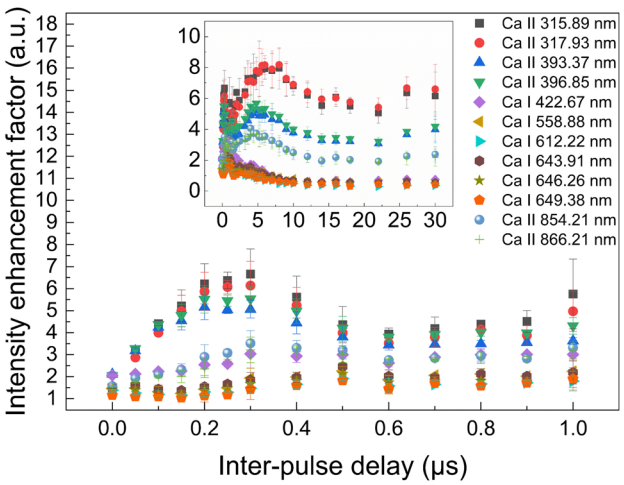

Fig. 6 The comparison of the intensity enhancement factor between the neutral and ionic calcium lines with increasing inter-pulse delay time.

higher enhancements than other metallic elements with a maximum enhancement of 5.2. However, the intensity enhancements of the Na I 589.59 nm and K I 769.90 nm lines were relatively lower than other lines. This might be due to the lower ionization energy of sodium and potassium resonance lines. The Na I 589.59 nm and K I 769.90 nm lines showed strong emission signals in single-pulse LIBS. The double-pulse configuration had less enhancement effect on the emission enhancement of the neutral lines of sodium and potassium.

3.4 Comparison of signal enhancement of neutral and ionic calcium lines

Finally, a comparative study of the intensity enhancement of the neutral and ionic calcium lines was carried out. There was a correlation between the signal enhancement and the upper energy level of the transition, as mentioned in other studies.[24–26] The intensity enhancement of the neutral and ionic calcium lines with increasing inter-pulse delay time is shown in Fig. 6 (with an energy ratio of 20 : 100), *i.e.* Ca II emitting at 315.89 nm, 317.933 nm, 393.37 nm, 396.85 nm, 854.21 nm, 866.21 nm and Ca I emitting at 422.67 nm, 558.88 nm, 612.22 nm, 643.91 nm, 646.26 nm and 649.38 nm. The enhancement curves of the ionic lines had two distinct peaks, while the curves of the neutral lines were relatively flat after 2 μs, and the intensity enhancement factors of the ionic lines were larger than those of the neutral lines. The two peak intensity enhancement factors of the Ca II 315.89 nm line were 6.7 and 8 with inter-pulse delay time of 0.3 μs and 8 μs, respectively, and the maximum intensity enhancement factor of the Ca I 558.88 nm line was 2.3 at 0.5 μs. The upper energy levels of the neutral and ionic calcium lines are shown in Table 1. It was found that the intensity enhancement factors of the ionic lines increased with the upper energy level. The upper energy level of Ca II 315.89 nm (7.047169 eV) and Ca II 317.93 nm (7.049551 eV) was much larger than that of the other four ionic lines, accompanied by a greater enhancement of the emission signal. Due to the higher excitation efficiency and the increased ablated mass by the second laser pulse, more atoms and molecules were excited into ions and the population of upper energy levels of the spectral lines increased, resulting in the signal emission of ionic lines with higher upper energy level being larger than other lines.[4] On the other hand, the maximum intensity enhancement factor of the neutral lines was much smaller than that of the ionic lines, although the upper energy level of Ca I 558.88 nm (4.743527 eV) was larger than that of Ca II 854.21 nm (3.150984 eV). This could be related to the larger ionization degree of the plasma.[24]

Table 1 shows that the enhancement factors of selected spectral lines varied from 1.31 to 8.18 times. The difference in signal enhancement could be attributed to the different spectroscopic parameters of the selected lines (*i.e.* energy levels) and the experimental conditions.

3.5 Excitation temperature and plasma lifetime

The plasma temperature and lifetime were calculated and observed to investigate the enhancement mechanism of collinear double-pulse LIBS. The plasma lifetime was obtained by measuring the line intensities against the detection delay time. The time evaluation of the normalized spectral line intensities in single-pulse LIBS and double-pulse LIBS (with the inter-pulse delay time of 0.2 μs and 6 μs, detection delay time after the second laser pulse of 0.8 μs) is shown in Fig. 7. The intensity was normalized to the range of 0–1. The emission signal of K I 769.90 nm lines lasted longer than other lines. Except for the K I 769.90 nm lines, the intensity of the H I 656.27 nm and O I 777.42 nm lines decreased drastically from 0 μs to 3 μs, and the C I 247.86 nm line decreased drastically from 0 μs to 5 μs. All lines gradually attenuated to background noise at about 15 μs. The double-pulse configuration effectively enhanced the emission signal of the coal plasma, although it had little effect on the plasma lifetime.

To better investigate the plasma properties, the plasma temperature was also calculated using the Boltzmann plot method. Assuming that the plasma is in local thermodynamic

 This journal is © The Royal Society of Chemistry 2023

Published on 26 June 2023. Downloaded by Zhejiang University on 11/8/2023 7:15:22 AM.

Table 1 The maximum intensity enhancement factors of selected spectral lines (at an energy ratio of 20 : 100)

Elemental species	Wavelength (nm)	E_i (eV)	E_k (eV)	Enhancement factor	Inter-pulse delay (μs)
C I	247.86	2.684014	7.684767	2.32	0.2
H I	656.27	10.198836	12.087505	3.42	8
O I	777.42	9.146091	10.740476	5.89	8
Fe II	259.94	0.000000	4.768307	2.89	6
Mg II	279.55	0.000000	4.433784	3.26	0.2
Na I	589.59	0.000000	2.102297	1.99	0.5
K I	769.90	0.000000	1.609958	1.31	0.9
Ca II	315.89	3.123349	7.047169	7.95	8
Ca II	317.93	3.150984	7.049551	8.18	8
Ca II	393.37	0.000000	3.150984	5.21	4.8
Ca II	396.85	0.000000	3.123349	5.69	4.8
Ca I	422.67	0.000000	2.932512	3.03	0.3
Ca I	558.88	2.525682	4.743527	2.25	0.5
Ca I	612.22	1.885808	3.910399	1.92	0.5
Ca I	643.91	2.525682	4.450647	2.46	0.5
Ca I	646.26	2.522987	4.440954	2.12	0.5
Ca I	649.38	2.521263	4.430012	1.82	0.5
Ca II	854.21	1.699932	3.150984	4.06	4
Ca II	866.21	1.692408	3.123349	3.70	4

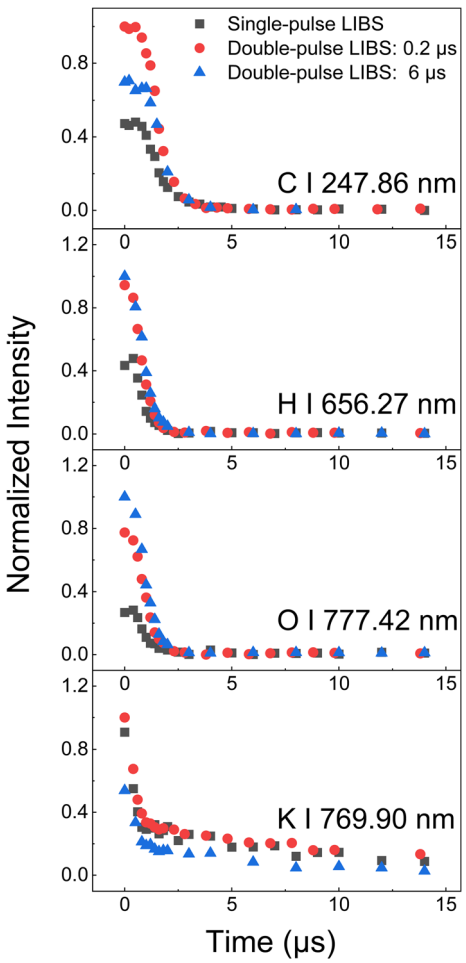

Fig. 7 Time evaluation of normalized intensities in single-pulse LIBS and double-pulse LIBS.

equilibrium (LTE), the plasma temperature can be estimated using the Boltzmann distribution function plot by the following equation:[27–29]

$$\ln\left(\frac{I\lambda}{gA}\right) = -\frac{E_k}{kT} + \ln\left(\frac{N(T)}{U(T)}\right) \quad (1)$$

I is the integral intensity and λ is the wavelength of the spectral line, g is the degeneracy of the upper energy level, A is the transition probability, k is the Boltzmann constant, T is the plasma temperature, E_k is the upper energy level, $N(T)$ is the total number density, F is constant depending on experimental conditions, $U(T)$ is the partition function. The plasma temperature can be calculated from the slope of the Boltzmann distribution plot. In this work, the spectral lines of Ca II emitting at 315.89 nm, 317.93 nm, 393.37 nm, 396.85 nm, 854.21 nm and 866.21 nm were used to obtain the plasma temperature, and the calculated values are shown in Fig. 8. The average plasma temperature of the single-pulse LIBS was about 10 100 K, shown as the red dashed line. With the energy ratio 80 : 40 and 60 : 60, the plasma temperature was lower with a larger error bar and there was an initial drop in plasma temperature in the range of 0–2 μs. As the energy of the first laser pulse was reduced from 60 mJ to 10 mJ, the plasma temperature curves shifted upwards and in most cases were above the dashed line. The temperature curves of 10 : 110, 20 : 100 and 40 : 80 showed a similar trend. In the curve of 20 : 100, there was an initial increase in plasma temperature from 9720 K to 11 325 K in the range of 0–0.2 μs, then it decreased to 10 500 K from 0.2 μs to 0.5 μs, and finally, it slightly increased to 12 300 K and remained constant in the range of 10–30 μs. As the energy of the first laser pulse was reduced to 5 mJ, the plasma temperature curve decreased and approached the dashed line. There was a strong positive correlation between the temperature curves and the intensity enhancement of the spectral lines. In general, the

Published on 26 June 2023. Downloaded by Zhejiang University on 11/8/2023 7:15:22 AM.

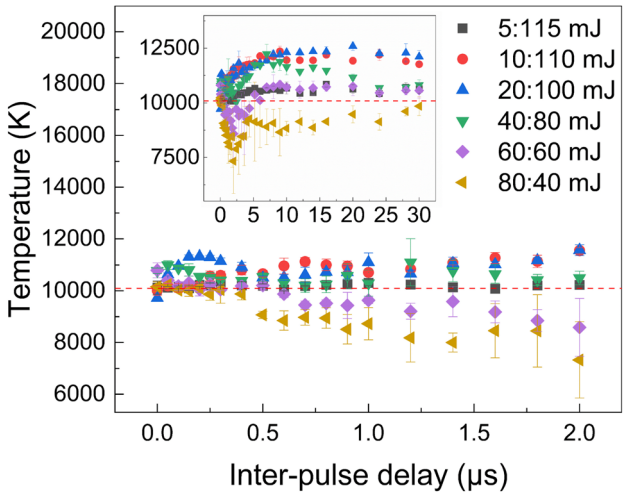

Fig. 8 Plasma temperature as a function of the inter-pulse delay time for different energy ratios.

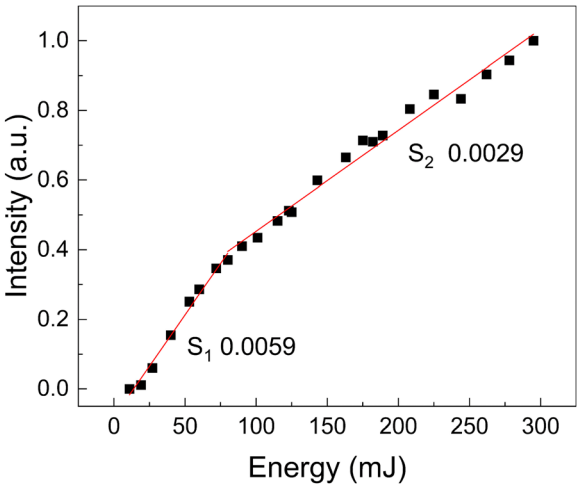

Fig. 9 Normalized intensity of C I 247.86 nm line using single-pulse LIBS (detection delay of 0.8 μs).

increase in plasma temperature was accompanied by an increase in the intensity of the spectral lines.

3.6 Emission enhancement mechanism in collinear double-pulse LIBS

The emission enhancement mechanism could be explained by the mechanism of the pulse–plasma coupling effect and the pulse–target interaction by combining the results of plasma lifetime and plasma temperature as a function of energy ratio and inter-pulse delay time.

For the energy ratios of 60 : 60 and 80 : 40, the intensity enhancement factor decreased with the inter-pulse delay time accompanied by a decrease in the plasma temperature in the range of 0–2 μs. The decrease in intensity enhancement and plasma temperature could be due to the second laser pulse being absorbed by the expanding front of the shock wave generated by the first laser pulse so that the second laser pulse could not interact efficiently with the sample. Fig. 9 shows the signal intensity of the C I 247.86 nm line as a function of pulse energy in single-pulse LIBS. The intensity increased almost linearly with laser energy, but more rapidly when the laser energy was at a low level. The slope of the fitted line was 0.0059 and 0.0029 for laser energy of 10–70 mJ and 70–300 mJ, respectively. The slope decreased rapidly when the laser pulse energy was greater than 70 mJ. This could be explained by the plasma shielding effect. At high laser intensity, part of the laser beam was absorbed and could not reach the sample surface, thus reducing the ablation efficiency to slow down the intensity increase.[30,31] After 2 μs the pre-plasma (generated by the first laser pulse) decayed, the shielding effect decreased and the coupling efficiency of the second laser pulse with the plasma plume increased, resulting in a higher plasma temperature and intensity enhancement.

As the energy of the first laser pulse decreased, two peaks of the intensity enhancement were found at the energy ratios of 10 : 110, 20 : 100 and 40 : 80. The signal enhancement could be attributed to both the improved coupling effect of the pre-plasma and the target with the second laser pulse.[32,33] The pre-plasma could be reheated and re-excited by the second laser pulse, resulting in a higher excitation efficiency of the ablated mass and an increased plasma temperature. On the other hand, the first laser pulse significantly influenced the environmental conditions of the interaction between the second laser pulse and the sample surface.[18] The ablation efficiency of the second laser pulse with the target was improved and the plasma expansion was facilitated by better environmental conditions

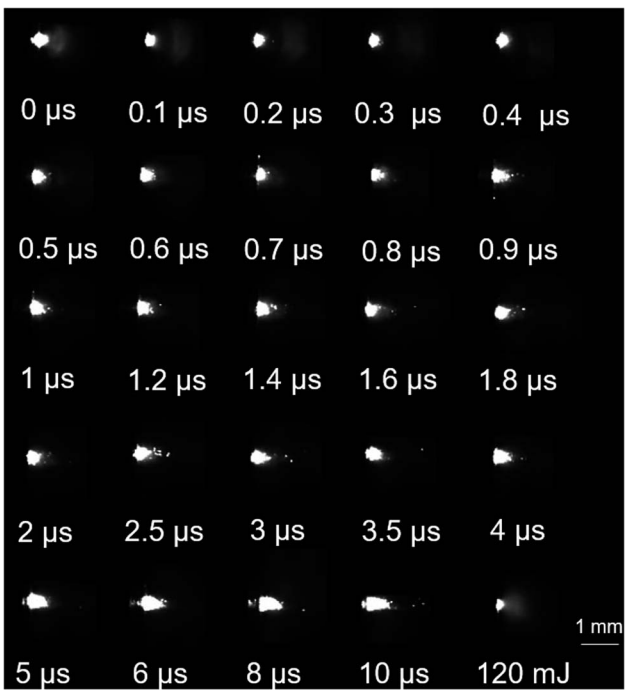

Fig. 10 Typical plasma images under different inter-pulse delay time. The images are recorded at the energy ratio of 20 : 100 and gate width of 10 μs.

This journal is © The Royal Society of Chemistry 2023

Published on 26 June 2023. Downloaded by Zhejiang University on 11/8/2023 7:15:22 AM.

(*i.e.* improved surface temperature and ambient rarefaction). The first peak could be attributed to the reheating and re-exciting effect of the second laser pulse with the pre-plasma and the larger ablated mass. By increasing the inter-pulse delay time, the density of the pre-plasma decreased significantly, resulting in a reduced coupling effect of the second laser pulse with the pre-plasma so that the enhancement decreased after the first peak.[16]

The fast image of the plasma in double-pulse LIBS with different inter-pulse delay time is shown in Fig. 10. The plasma images were obtained by using a high-speed digital camera (Y4-S1, IDT) equipped with a Nikon lens (200 mm, f/4.0 Micro). As shown in Fig. 10, a stable plasma with a relatively round core can be observed in the range of 0–2 μs. However, as the inter-pulse delay time increased to 2 μs, the plasma tended to become larger with an elongated irregular core. The second peak in the intensity enhancement curve was most likely due to a larger ablated mass and plasma expansion in a better environmental condition, resulting in a larger plasma with a higher temperature. Although the energy of the first laser pulse was 5 mJ and could not ablate the target and generate a plasma, the signal enhancement was also observed contributing to the conditions changed by the first laser pulse.[33]

4. Conclusions

In this work, the emission signal enhancement of coal plasma has been observed by employing the collinear double-pulse LIBS. The intensity enhancement factor of C I 247.86 nm, H I 656.27 nm and O I 777.42 nm lines as a function of inter-pulse delay time was investigated with different energy ratios changing from 5 : 115 (E_1 = 5 mJ and E_2 = 115 mJ) to 80 : 40 (E_1 = 80 mJ and E_2 = 40 mJ). Better enhancement was achieved when the energy of the first laser pulse was lower than that of the second laser pulse (*i.e.* energy ratios of 10 : 110 and 20 : 100). With the optimized energy ratio fixed at 20 : 100, the intensity enhancement of metallic and alkali element lines was also observed and the maximum intensity enhancement factor varied from 1.31 to 8.18. Moreover, the intensity enhancement factors of the ionic calcium lines were stronger than that of the neutral lines. The intensity enhancement of the spectral line of Ca II 315.89 nm was obtained to be 8 with an inter-pulse delay time of 8 μs, almost three times greater than that of Ca I 643.91 nm. The intensity enhancement of the selected spectral lines could be explained by the pre-plasma plume reheating, plasma expansion and higher ablation efficiency, resulting in a larger plasma and higher plasma temperature. These results illustrate the potential of collinear double-pulse LIBS for simultaneous multi-element detection of coal.

Conflicts of interest

There are no conflicts of interest to declare.

Acknowledgements

This project was supported by Zhejiang Provincial Natural Science Foundation of China (LZ21E060003, LR23E060001) and the Fundamental Research Funds for the Central Universities (2022ZFJH004).

References

1 T. Yuan, Z. Wang, S.-L. Lui, Y. Fu, Z. Li, J. Liu and W. Ni, *J. Anal. At. Spectrom.*, 2013, **28**, 1045–1053.
2 S. Sheta, M. S. Afgan, Z. Hou, S.-C. Yao, L. Zhang, Z. Li and Z. Wang, *J. Anal. At. Spectrom.*, 2019, **34**, 1047–1082.
3 K. Liu, C. He, C. Zhu, J. Chen, K. Zhan and X. Li, *TrAC, Trends Anal. Chem.*, 2021, **143**, 116357.
4 V. I. Babushok, F. C. DeLucia, J. L. Gottfried, C. A. Munson and A. W. Miziolek, *Spectrochim. Acta, Part B*, 2006, **61**, 999–1014.
5 Y. H. Jiang, R. H. Li and Y. Q. Chen, *Spectrochim. Acta, Part B*, 2021, **186**, 106321.
6 X. Mao, X. Zeng, S.-B. Wen and R. E. Russo, *Spectrochim. Acta, Part B*, 2005, **60**, 960–967.
7 R. Yang and L. Bi, *Optik*, 2021, **243**, 167025.
8 L. B. Guo, Z. Q. Hao, M. Shen, W. Xiong, X. N. He, Z. Q. Xie, M. Gao, X. Y. Li, X. Y. Zeng and Y. F. Lu, *Opt. Express*, 2013, **21**, 18188–18195.
9 S. Zhao, X. Gao, A. Chen and J. Lin, *Appl. Phys. B: Lasers Opt.*, 2019, **126**, 7.
10 J. Viljanen, Z. Sun and Z. T. Alwahabi, *Spectrochim. Acta, Part B*, 2016, **118**, 29–36.
11 Y. Liu, M. Baudelet and M. Richardson, *J. Anal. At. Spectrom.*, 2010, **25**, 1316–1323.
12 A. Khumaeni, T. Motonobu, A. Katsuaki, M. Masabumi and W. Ikuo, *Opt. Express*, 2013, **21**, 29755–29768.
13 M. Tampo, M. Miyabe, K. Akaoka, M. Oba, H. Ohba, Y. Maruyama and I. Wakaida, *J. Anal. At. Spectrom.*, 2014, **29**, 886–892.
14 A. J. Effenberger and J. R. Scott, *Anal. Bioanal. Chem.*, 2011, **400**, 3217–3227.
15 D. Sun, Y. Ma, Y. Wang, M. Su, Q. Lu and C. Dong, *Anal. Methods*, 2018, **10**, 2595–2603.
16 I. Y. Elnasharty, F. R. Doucet, J. F. Y. Gravel, P. Bouchard and M. Sabsabi, *J. Anal. At. Spectrom.*, 2014, **29**, 1660–1666.
17 Y. Li, D. Tian, Y. Ding, G. Yang, K. Liu, C. Wang and X. Han, *Appl. Spectrosc. Rev.*, 2018, **53**, 1–35.
18 E. Tognoni and G. Cristoforetti, *J. Anal. At. Spectrom.*, 2014, **29**, 1318–1338.
19 A. De Giacomo, M. Dell'Aglio, D. Bruno, R. Gaudiuso and O. De Pascale, *Spectrochim. Acta, Part B*, 2008, **63**, 805–816.
20 P. K. Diwakar, S. S. Harilal, J. R. Freeman and A. Hassanein, *Spectrochim. Acta, Part B*, 2013, **87**, 65–73.
21 G. Nicolodelli, G. S. Senesi, R. A. Romano, I. L. de Oliveira Perazzoli and D. M. B. P. Milori, *Spectrochim. Acta, Part B*, 2015, **111**, 23–29.
22 Y. Ma, W. Zhang, Z. Xiong, H. Cui, Q. Li, R. Zhou, Y. Zhang, X. Li, X. Zeng and Q. Li, *J. Anal. At. Spectrom.*, 2020, **35**, 1458–1463.
23 S. Legnaioli, B. Campanella, S. Pagnotta, F. Poggialini and V. Palleschi, *Spectrochim. Acta, Part B*, 2019, **155**, 123–126.
24 L. St-Onge, V. Detalle and M. Sabsabi, *Spectrochim. Acta, Part B*, 2002, **57**, 121–135.

Published on 26 June 2023. Downloaded by Zhejiang University on 11/8/2023 7:15:22 AM.

25 S. M. A. Jon Scaffidi and D. A. Cremers, *Anal. Chem.*, 2006, **78**, 24–32.
26 P. A. Benedetti, G. Cristoforetti, S. Legnaioli, V. Palleschi, L. Pardini, A. Salvetti and E. Tognoni, *Spectrochim. Acta, Part B*, 2005, **60**, 1392–1401.
27 W. P. Xu, A. M. Chen, Q. Y. Wang, D. Zhang, Y. Wang, S. Y. Li, Y. F. Jiang and M. X. Jin, *J. Anal. At. Spectrom.*, 2019, **34**, 1018–1025.
28 N. Idris, T. N. Usmawanda, K. Lahna and M. Ramli, *J. Phys.: Conf. Ser.*, 2018, **1120**, 012098.
29 P. Stavropoulos, A. Michalakou, G. Skevis and S. Couris, *Spectrochim. Acta, Part B*, 2005, **60**, 1092–1097.
30 G. Yang, Q. Lin, Y. Ding, D. Tian and Y. Duan, *Sci. Rep.*, 2015, **5**, 7625.
31 S. Nammi, N. J. Vasa, B. Gurusamy and A. C. Mathur, *J. Phys. D: Appl. Phys.*, 2017, **50**, 355204.
32 I. Y. Elnasharty, F. R. Doucet, J.-F. Y. Gravel, P. Bouchard and M. Sabsabi, *J. Anal. At. Spectrom.*, 2014, **29**, 1660–1666.
33 N. Li, E. Harefa and W. Zhou, *Plasma Sci. Technol.*, 2022, **24**, 115507.

This journal is © The Royal Society of Chemistry 2023